PCCP

Kinetics of Interfacial Curing Reaction for an Epoxy-Amine Mixture

Journal:	*Physical Chemistry Chemical Physics*
Manuscript ID	CP-COM-07-2022-003394
Article Type:	Communication
Date Submitted by the Author:	24-Jul-2022
Complete List of Authors:	Yamaguchi, Ko; Kyushu University, Applied Chmistry Kawaguchi, Daisuke; Kyushu University, Applied Chmistry Miyata, Noboru; Comprehensive Research Organisation for Science and Society Research Center for Neutron Science and Technology Miyazaki, Tsukasa; Comprehensive Research Organisation for Science and Society Research Center for Neutron Science and Technology Aoki, Hiroyuki; Japan Atomic Energy Agency, J-PARC Center; High Energy Accelerator Research Organisation, Institute of Materials Structure Science Yamamoto, Satoru; Kyushu University, Center for Polymer Interface and Molecular Adhesion Science Tanaka, Keiji; Kyushu University, Applied Chemistry

COMMUNICATION

Kinetics of Interfacial Curing Reaction for an Epoxy-Amine Mixture

Ko Yamaguchi[a], Daisuke Kawaguchi[a,b*], Noboru Miyata[c], Tsukasa Miyazaki[c], Hiroyuki Aoki[d,e], Satoru Yamamoto[b], and Keiji Tanaka[a,b*]

Received 00th January 20xx,
Accepted 00th January 20xx

DOI: 10.1039/x0xx00000x

A better understanding of the chemical reaction between epoxy and amine compounds at a solid interface is crucial for the design and fabrication of materials with appropriate adhesive strength. Here, we examined the curing reaction kinetics of epoxy phenol novolac and 4,4'-diaminodiphenyl sulfone at the outermost interface using sum-frequency generation spectroscopy, X-ray and neutron reflectivity in conjunction with a full atomistic molecular dynamics simulation. The reaction rate constant was much larger at the quartz interface than in the bulk. While the apparent activation energy at the quartz interface obtained from an Arrhenius plot was almost identical to the bulk value, the frequency factor at the quartz interface was greater than that in the bulk. These results could be explained in terms of the densification and orientation of reactants at the interface, facilitating the encounter of the reactants present.

Epoxy resins, which are obtained by curing reactions between an epoxy base and hardener compounds, are an important class of thermosetting polymers used in various applications such as structural materials, encapsulants, and adhesives[1-4]. The mechanical properties of these resins strongly depend on the characteristics of the three-dimensional network structure, which are governed by how the chemical reaction proceeds within it[5-8]. Thus, when considering epoxy resin adhesive applications, it should be better understood how the curing reactions proceed on the adherend surface as the first benchmark. Reaction kinetics between epoxy and amine compounds near a solid surface have been hitherto studied using Fourier transform infrared spectroscopy (FT-IR)[9-11]. FT-IR imaging has revealed that the reaction between bisphenol-A diglycidyl ether (DGEBA) and ethylenediamine (EDA) becomes slower in close proximity to the surface of silane-coated glass fibers[9]. In an earlier study, we applied with an attenuated total reflection mode (ATR-FT-IR), in which the depth resolution is in several hundreds of nanometers, to study the reaction kinetics of a model system composed of phenyl glycidyl ether (PGE) and hexylamine (HA)[10], and found that the curing reaction was slower at the interface than in the bulk. The slower reaction kinetics could be explained in terms of the lesser mobility of reactants due to the presence of the interface. On the other hand, another study found that the curing reaction between DGEBA and aniline was faster in nanoconfined anodic aluminum oxide (AAO) pores than in the bulk.[11]. Although this initially appears to be inconsistent with the earlier examples, the interfacial effect could have been more greatly emphasized in the latter case.

Sum-frequency generation (SFG) spectroscopy is a type of vibrational spectroscopy based on the second-order nonlinear optical effect[12, 13]. Thus, SFG signals can be generated only from places where the centrosymmetry is broken, or more generally, the interfaces[14-25]. This means that using SFG, the curing reaction between epoxy and amine compounds can be monitored at the interface with a depth region at the molecular level. The objective of this study was to examine the kinetics of the curing reaction between epoxy phenol novolac (EPN) and 4,4'-diaminodiphenyl sulfone (DDS) at a quartz interface using SFG spectroscopy in conjunction with a full atomistic molecular dynamics (MD) simulation. The results obtained should help to provide a better understanding of the curing reaction of epoxy and amine, especially the kinetic gradient, if any, in close proximity to the adherent surface.

Figure 1 shows chemical structures of EPN and DDS, which were kindly supplied by DIC Corporation, Japan, and purchased from Tokyo Chemical Industry Co. Japan, respectively. The epoxy equivalent weight of EPN was 187 g•mol^{-1}. Quartz plates

[a] Department of Applied Chemistry, Kyushu University, Fukuoka 819-0395, Japan
[b] Center for Polymer Interface and Molecular Adhesion Science, Kyushu University, Fukuoka 819-0395, Japan
[c] Neutron Science and Technology Center, Comprehensive Research Organization for Science and Society, 162-1 Shirakata, Tokai, Naka, Ibaraki 319-1106, Japan
[d] Materials and Life Science Division, J-PARC Center, Japan Atomic Energy Agency, 2-4 Shirakata, Tokai, Ibaraki 319-1195, Japan
[e] Institute of Materials Structure Science, High Energy Accelerator Research Organization, 203-1 Shirakata, Tokai, Naka, Ibaraki 319-1106, Japan

† Footnotes relating to the title and/or authors should appear here.
Electronic Supplementary Information (ESI) available: [details of any supplementary information available should be included here]. See DOI: 10.1039/x0xx00000x

and silicon wafers with a native oxide layer were used as substrates. They were cleaned in a piranha solution at 373 K for 2 h prior to use. The thermal properties of EPN and DDS were examined by differential scanning calorimetry (DSC) with a heating rate of 10 K•min^{-1} using a DSC 6220 (Hitachi High-Tech Science Co., Tokyo, Japan). The glass transition temperature (T_g) for EPN was 296 K, and the melting temperature (T_m) for DDS was 450 K. The mass density of well-cured EPN/DDS was observed to be 1.28 g•cm^{-3} by gas pycnometer (ULTRAPYC 1200e [Quantachrome Instruments Inc., Boynton Beach, FL, USA]) with a helium probe at 296 K. EPN and DDS were stoichiometrically dissolved in tetrahydrofuran (THF), and the solution was then cast onto a quartz substrate with a 15 μm-thick spacer. To prepare a sandwiched film, another quartz substrate was placed on it and it was then dried under vacuum at 353 K for 12 h to remove the residual solvent.

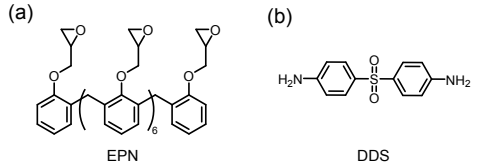

Figure 1. Chemical structure of (a) EPN and (b) DDS.

The curing reaction in the bulk was examined by an FT/IR-620 spectrometer (JASCO Corporation, Tokyo, Japan) with a triglycine sulfate (TGS) detector. Spectra were collected at temperatures ranging from 373 to 403 K with a resolution of 4 cm^{-1} and 64 scans. The corresponding interfacial reaction is discussed on the basis of SFG spectroscopy (EKSPLA, Vilnius, Lithuania). A visible beam with a wavelength of 532 nm and a tunable IR beam were introduced to a specimen with an incident angle of 65° and 55° relative to the substrate normal, respectively. The SFG measurements were carried out at the corresponding temperatures to those of FT-IR using the *ssp* (SFG/*s*; visible/*s*; and IR/*p*) polarization combination, meaning that the vibrational information along the direction normal to the interface was obtained. For the kinetic analysis, the time-dependent SFG measurement at a fixed wavenumber was conducted. The intensity of SFG signal (I^{SFG}) is proportional to the square of the effective sum-frequency susceptibility tensor of the interface ($\chi^{(2)}_{eff}$),

$$I^{SFG} \propto \left|\chi^{(2)}_{eff}\right|^2 \cdot I_{vis} \cdot I_{IR} \quad (1)$$

where I_{vis} and I_{IR} are the intensity of the incident visible and IR beams, respectively. Note that the $|\chi^{(2)}_{eff}|$ is proportional to the number density of functional groups of interest. The density profile of the EPN/DDS film along the normal direction was examined by X-ray reflectivity (XR) measurement using a SmartLab (Rigaku Corporation, Tokyo, Japan). The light source and detector were CuKα (λ = 0.154 nm) and a scintillation counter, respectively. XR curves were analyzed using Motofit software[26].

An MD simulation of the epoxy and amine mixture at the quartz interface was also performed[27]. A simulation system was considered in which an equivalent mixture of 400 EPNs and 800 DDSs was sandwiched between two layers of quartz [100] terminated with OH groups via periodic boundary conditions. The thickness of the quartz substrate was 2.1 nm, and the whole model size was 8.5×8.4×15.8 nm^3. A 1 ns MD simulation was performed at 403 K to obtain a detailed molecular picture near the quartz interface. The Forcite module of Materials Studio 2021 (Dassault Systèmes) with the COMPASS III force field was used for the simulation.

Panels (a) and (b) of Figure 2 show typical FT-IR and SFG spectra for EPN/DDS at 403 K as a function of curing time, corresponding to the bulk and interface, respectively. For clarity, each spectrum has been vertically shifted. In the region of 3,200 to 3,600 cm^{-1}, peaks at 3,370 and 3,476 cm^{-1} were assignable to the symmetric and anti-symmetric stretching modes of amine groups (NH_2s and NH_2as)[28]. Also, the stretching vibration mode of hydroxy groups (OHs) appeared in the range from 3,400 to 3,600 cm^{-1} as a broad peak. The absorbance for NH_2s and NH_2as decreased with increasing time. The SFG intensity for NH_2s also decreased with increasing time.

In the case of SFG spectroscopy, signals from functional groups of interest can be detected only when the functional groups are oriented at the interface. Hence, the above-mentioned decay of the SFG NH_2s peak implies either a reduction of the interfacial orientation of NH_2 groups or a decrease in the number of NH_2 groups at the interface. The former and latter correspond to the orientational relaxation by the thermal treatment and curing reaction with EPN, respectively. To address which is more plausible, SFG measurement for a homo DDS film sandwiched with quartz substrates was conducted at 403 K as a function of time, as shown in Figure S1. In contrast to EPN/DDS, the SFG intensity for NH_2s remained almost constant with increasing time for the DDS film. This confirms that the orientational relaxation of NH_2 groups at the interface should be minimal or non-existent under the current condition. Thus, it seems reasonable to consider that the time decay of the SFG NH_2s peak at 403 K, shown in Figure 2(b), reflects the progress in the reaction of DDS with EPN.

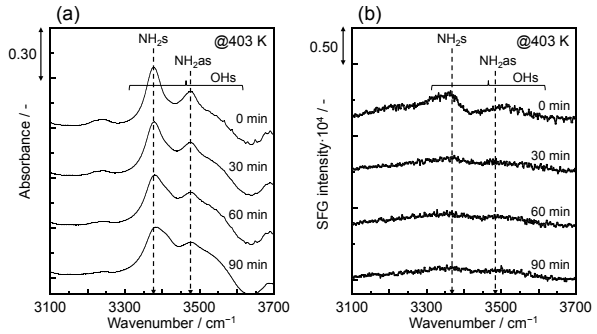

Figure 2. (a) FT-IR and (b) SFG spectra for EPN/DDS cured at 403 K as a function of time.

The reaction kinetics in the bulk and at the interface were analyzed. Since the IR absorbance is simply proportional to the number density of functional groups in a film, as expressed by the Lambert-Beer law, a decrease in the absorbance reflects the consumption of amino groups. On the other hand, as shown in eq. (1), a decrease in the square root of the I^{SFG} ($\sqrt{I^{SFG}}$) reflects

the consumption of amino groups at the interface. Figure 3(a) shows the time dependence of NH_2s absorbance by FT-IR (A^{IR}, left-hand side of Y axis) and the square root of SFG signal intensity ($\sqrt{I^{SFG}}$, right-hand side of Y axis) for EPN/DDS-2/1 at 403 K. Here, the A^{IR} and $\sqrt{I^{SFG}}$ were the peak-top values at 3,370 cm^{-1}, and $\sqrt{I^{SFG}}$ was acquired from the time-dependent measurement mode at the wavenumber. Filled triangles were imported from the SFG spectra shown in Figure 2(b). Although both A^{IR} and $\sqrt{I^{SFG}}$ decreased with time, these decreases were clearly different from each other. Assuming that the curing reaction between epoxy and amine at the initial stage is the first-order, A^{IR} and $\sqrt{I^{SFG}}$ can be expressed as:

$$A^{IR} \text{or} \sqrt{I^{SFG}} = \mathrm{a}\cdot\exp\left(\frac{-t}{\tau}\right) + \mathrm{b} \qquad (2)$$

where t and τ are the curing time and time constant, respectively, and a and b are constants. Solid curves denote the best-fits using eq. (2) and a = 0.16, b = 0.16 and $\tau = 1.48 \times 10^2$ min for the bulk, and a = 2.50×10^{-3}, b = 8.13×10^{-3} and $\tau = 2.91 \times 10^1$ min for the interface. Since the τ value was smaller at the interface than that in the bulk, it can be claimed that the reaction proceeded faster at the interface.

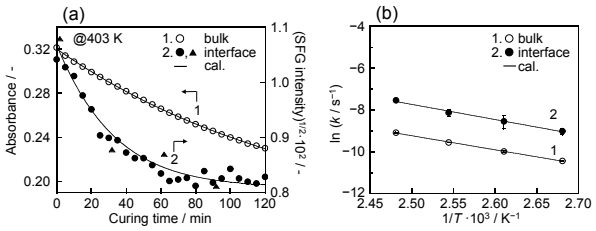

Figure 3. (a) Time dependence of A^{IR} and $\sqrt{I^{SFG}}$ for EPN/DDS at 403 K. Filled triangles correspond to SFG signals in Figure 2(b). (b) Arrhenius plot of k for EPN/DDS in the bulk and at the outermost interface. Solid lines denote the best-fit using an Arrhenius equation.

The apparent reaction rate constant (k) at the initial stage can be given by the reciprocal number of τ. Figure 3(b) shows the relationships between the reciprocal temperature and k. The relationships both in the bulk and at the interface looked to be fitted by a straight line. Thus, the following Arrhenius equation was applied to the data sets:

$$\ln k = -\frac{E_a}{RT} + \ln A \qquad (3)$$

where E_a, R, T, and A are the activation energy, gas constant, absolute temperature, and frequency factor, respectively. Solid lines denote the best-fits using eq. (3). The E_a values obtained from the linear slopes in Figure 3 (b) for the bulk and interface were (56.1±1.2) and (60.2±3.9) kJ•mol^{-1}, respectively. Here, errors denote standard deviations for the fitting of the Arrhenius analysis. This means that the energy barrier for the chemical reaction at the interface was almost identical to that in the bulk. On the other hand, the A values obtained from the intercepts in Figure 3(b) for the bulk and interface were (2.08±0.10) × 10^3 and (3.22±0.75) × 10^4, respectively. Therefore, the interfacial value was 15.7 times greater than in the bulk.

Even in a binary miscible mixture, a component is segregated at an interface to minimize the free energy[29]. This is the case for systems composed of epoxy and amine mixtures. Although the segregation is controlled by the balance between enthalpic and entropic factors, in the case of the epoxy and amine mixture, the component with a smaller size is supposed to be generally segregated at the interface thanks to the gain in packing and/or translational entropy unless there is a clear difference in cohesive energy between the components[30]. Since a DDS molecule is smaller than an EPN molecule, it can be expected that DDS is preferentially segregated at the interface. The segregation effect of DDS on the reaction kinetics is discussed in the following.

If the local concentration of DDS is higher at the interface than in the bulk, the consumption rate of DDS itself is supposed to become faster. However, the k value itself should remain unchanged as long as the E_a and A values are unchanged. Panels (a) and (b) of Figure S2 show the E_a and A values obtained from an Arrhenius analysis of the EPN/DDS system with mixing ratios of 1:1 and 3:1. It was clear that both values were independent of the mixing rate not only in the bulk but also at the interface. This result indicates that the interfacial segregation of DDS cannot be a dominant factor in the greater k value observed for the curing reaction at the interface.

Other plausible explanations for the greater k value at the interface shown in Figure 3(b) are a more favorable orientation and/or densification of reactants there. As seen in the phenomenon of interfacial freezing where a crystalline monolayer can survive even at a temperature above the bulk melting temperature by 2~3 K [31-33], organic molecules tend to be aligned at the interface with a better ordering than the bulk. Also, for polymer films, it has been reported that the mass density near the substrate interface could be higher than that in the internal region of the film[34-40].

To gain an insight into the molecular picture of the EPN/DDS system at the interface, an MD simulation was conducted. Figure 4(a) shows the depth profile of mass density for the mixture. The mass density was approximately 1.5 times higher at the interface than in the internal region. Figure 4(b) shows the relative number density of epoxy oxygen and amine nitrogen atoms as a function of the distance from the interface. Although they were approximately 2 and 1 in the interior region, respectively, as expected from the stoichiometric ratio, the magnitude relationship was reversed at the quartz interface, meaning that DDS was segregated at the quartz interface as previously mentioned. In addition, amine molecules were oriented at the interface along the parallel direction. Figure 4(c) shows the distribution of the order parameter (S) given by (1/2)·{3($\boldsymbol{n}\cdot\boldsymbol{a}_z$)^2-1}, where $\boldsymbol{n}$ is a unit vector parallel to a phenyl group of a DDS molecule shown in the inset, $\boldsymbol{a}_z$ is a unit vector normal to the solid surface. Here, an S of approximately -0.5 indicates that phenyl groups of DDS are oriented along the direction parallel to the interface. A peak observed near 0.3 nm from the interface was due to phenyl groups attached to DDS in the opposite direction to the phenyl groups oriented at the outermost interface. It should be noted here that a DDS molecule is not planar in shape due to bonds from the central sulfur toward the apex direction of the tetrahedron. Figure 4(d) shows a representative snapshot of DDS molecules present at the interface. In most DDS molecules,

one phenyl group was attached with the plane to the substrate surface, i.e. oriented along the direction parallel to the substrate, and other groups were somehow oriented along the diagonal direction from the substrate surface.

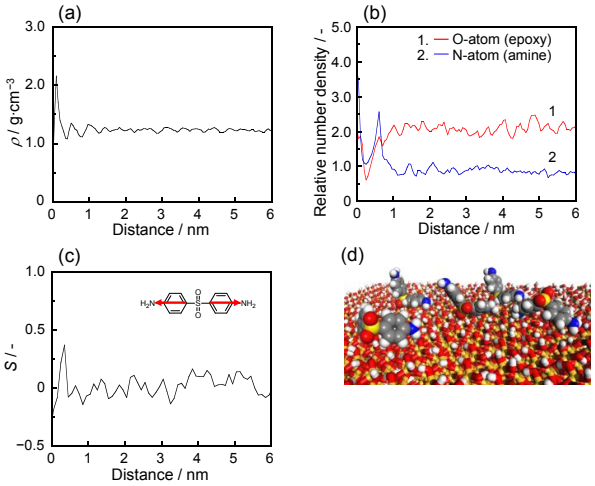

Figure 4. (a) Density profile of an EPN/DDS mixture along the direction normal to the substrate interface. (b) Depth profiles of mass density for epoxy oxygen and amine nitrogen atoms. (c) Depth dependence of *S* for an EPN/DDS mixture. (d) Atomistic model of DDS molecules at the quartz interface. White, gray, red, blue and yellow spheres denote hydrogen, carbon, oxygen, nitrogen and silicon atoms, respectively.

To verify experimentally the interfacial densification, XR measurement was conducted. An EPN/DDS thin film on a silicon substrate dried at 353 K for 12 h, which was the same condition as the sample for the SFG measurements before starting curing, was used. Figure 5(a) shows an XR profile for the EPN/DDS film. Open symbols correspond to the experimental data. Black and red curves denote calculated reflectivity obtained from one- and two-layer models expressed by black and red model density profiles shown in Figure 5(b). The former and latter are models without/with the interfacial densification layer of 0.6 nm. The two-layer model was basically created by averaging the density in the interface region as a result of the MD simulation shown in Fig. 4 (a). The inset of Figure 5(b) shows the enlarged profile near the quartz interface. The χ^2 values for the fitting analysis using the one- and two-layer models were 6.15 and 4.86, respectively. This means that the two-layer model exhibited better reflectivity than the one-layer model. Thus, it is most likely that the densification occurred at the solid interface.

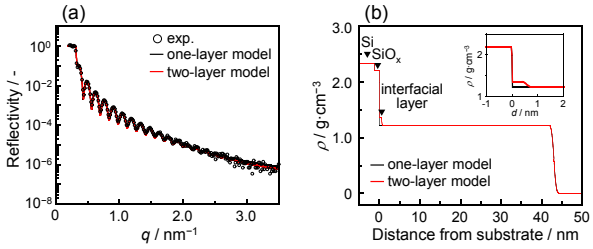

Figure 5. (a) An XR curve for a cured EPN/DDS film on a silicon substrate. Symbols and solid curves denote, respectively, an experimental data set and calculated reflectivity based on model density profiles shown in (b).

Previously, using ATR-FT-IR, we reported that the curing reaction for a model epoxy system was slower in the interfacial region than in the bulk because of the lesser mobility of reactants[10]. The main difference between ATR-FT-IR and the current SFG analysis is the depth region where the information is collected. This makes it clear that there is a conversion gradient in close proximity to the quartz interface along the normal direction. To confirm this hypothesis, the EPN/DDS film on the quartz substrate was partially cured at 403 K for 30 min and then leached using THF. XR and neutron reflectivity measurements detected an insoluble EPN/DDS layer with a thickness of ca. 5 nm on the substrate (not shown). On the other hand, such a residual layer on the substrate was not discerned without the partial curing reaction. Thus, it is conceivable that the curing reaction of epoxy slows down from the bulk region toward the adherent surface but speeds up at the outermost interface. This can be explained in terms of the enhanced collision frequency of epoxy and amine groups due to interfacial densification and orientation. A detailed and quantitative picture of the interfacial curing reactions is currently under consideration.

Conclusions

The initial curing kinetics of EPN/DDS in the bulk and at the outermost quartz interface were examined by FT-IR and SFG spectroscopy, respectively. The curing rate at the outermost interface was higher than that in the bulk at a given temperature. Although there was no difference in the activation energy of the reaction between the bulk and interface, the frequency factor was greater at the interface than in the bulk. MD simulation revealed that at the outermost quartz interface, amino groups were well oriented and the mass density increased in comparison with the bulk. Thus, the faster reaction at the outermost inter-face can be explained in terms of the densification and orientation of reactive functional groups. These findings will be helpful for a better understanding and design of nanocomposites and adhesives using thermosetting polymers.

Conflicts of interest

There are no conflicts to declare.

Acknowledgements

We are grateful to DIC Corporation for kindly providing EPN. This work was supported by JSPS KAKENHI for Scientific Research (B) (No. JP20H02790) to KT and Scientific Research (B) (No. JP20H02802) to DK from the Ministry of Education, Culture, Sports, Science, and Technology (MEXT), Japan. We are also thankful for the support from the JST-Mirai Program (JPMJMI18A2) (K.T.). NR measurements were performed at BL17 SHARAKU at MLF, J-PARC (No. 2019L0603).

Notes and references

1. F.-L. Jin, X. Li and S.-J. Park, *J. Ind. Eng. Chem.*, 2015, **29**, 1-11.
2. N. Domun, H. Hadavinia, T. Zhang, T. Sainsbury, G. H. Liaghat and S. Vahid, *Nanoscale*, 2015, **7**, 10294-10329.
3. R. Aoki, A. Yamaguchi, T. Hashimoto, M. Urushisaki, T. Sakaguchi, K. Kawabe, K. Kondo and H. Iyo, *Polym. J.*, 2019, **51**, 909-920.
4. A. Hanafusa, S. Ando, S. Ozawa, M. Ito, R. Hasegawa, K. Mayumi and K. Ito, *Polym. J.*, 2020, **52**, 1211-1221.
5. T. D. Chang, S. H. Carr and J. O. Brittain, *Polym. Eng. Sci.*, 1982, **22**, 1213-1220.
6. M. Aoki, A. Shundo, S. Yamamoto and K. Tanaka, *Soft Matter*, 2020, **16**, 7470-7478.
7. A. Shundo, M. Aoki, S. Yamamoto and K. Tanaka, *Macromolecules*, 2021, **54**, 5950-5956.
8. A. Shundo, M. Aoki, S. Yamamoto and K. Tanaka, *Macromolecules*, 2021, **54**, 9618-9624.
9. J. González-Benito, *J. Colloid Interface Sci.*, 2003, **267**, 326-332.
10. T. Hirai, K. Kawasaki and K. Tanaka, *Phys. Chem. Chem. Phys.*, 2012, **14**, 13532-13534.
11. M. Tarnacka, M. Dulski, S. Starzonek, K. Adrjanowicz, E. U. Mapesa, K. Kaminski and M. Paluch, *Polymer*, 2015, **68**, 253-261.
12. Y. R. Shen, *Nature*, 1989, **337**, 519-525.
13. Z. Chen, Y. R. Shen and G. A. Somorjai, *Annu. Rev. Phys. Chem.*, 2002, **53**, 437-465.
14. S. Ye, Y. J. Tong, A. M. Ge, L. Qiao and P. B. Davies, *Chem. Rec.*, 2014, **14**, 791-805.
15. H. Zhu, N. Dhopatkar and A. Dhinojwala, *ACS Macro Lett.*, 2016, **5**, 50-54.
16. I. Chae, S. Ahmed, H. B. Atitallah, J. Luo, Q. Wang, Z. Ounaies and S. H. Kim, *Macromolecules*, 2017, **50**, 2838-2844.
17. H. K. Nguyen, M. Inutsuka, D. Kawaguchi and K. Tanaka, *J. Chem. Phys.*, 2017, **146**, 203313.
18. H. Noguchi and K. Uosaki, in *Nanolayer Research*, ed. T. Imae, Elsevier, Amsterdam, 2017, DOI: https://doi.org/10.1016/B978-0-444-63739-0.00006-2, pp. 203-241.
19. S. Sugimoto, M. Inutsuka, D. Kawaguchi and K. Tanaka, *ACS Macro Lett.*, 2018, **7**, 85-89.
20. S. Singla, G. Amarpuri, N. Dhopatkar, T. A. Blackledge and A. Dhinojwala, *Nat. Commun.*, 2018, **9**, 1890.
21. H. K. Nguyen, S. Sugimoto, A. Konomi, M. Inutsuka, D. Kawaguchi and K. Tanaka, *ACS Macro Lett.*, 2019, **8**, 1006-1011.
22. T. Lin, Y. Wu, E. Santos, X. Chen, D. Ahn, C. Mohler and Z. Chen, *Langmuir*, 2020, **36**, 15128-15140.
23. B. L. Li, J. S. Andre, X. Y. Chen, B. Walther, R. Paradkar, C. Feng, C. Tucker, C. Mohler and Z. Chen, *Anal. Chem.*, 2020, **92**, 14145-14152.
24. Q. Xu, N. Zhu, H. Fang, X. Wang, R. D. Priestley and B. Zuo, *ACS Macro Lett.*, 2021, **10**, 1-8.
25. B. Zuo, C. Li, Q. Xu, K. Randazzo, N. Jiang, X. Wang and R. D. Priestley, *ACS Nano*, 2021, **15**, 9568-9576.
26. A. Nelson, *J. Appl. Crystallogr.*, 2006, **39**, 273-276.
27. S. Yamamoto, R. Kuwahara, M. Aoki, A. Shundo and K. Tanaka, *ACS Appl. Polym. Mater.*, 2020, **2**, 1474-1481.
28. H. Wang, Y. Zhang, L. Zhu, Z. Du, B. Zhang and Y. Zhang, *Thermochim. Acta*, 2011, **521**, 18-25.
29. D. Kawaguchi, K. Tanaka, N. Torikai, A. Takahara and T. Kajiyama, *Langmuir*, 2007, **23**, 7269-7275.
30. S. Yamamoto and K. Tanaka, *Soft Matter*, 2021, **17**, 1359-1367.
31. X. Z. Wu, E. B. Sirota, S. K. Sinha, B. M. Ocko and M. Deutsch, *Phys. Rev. Lett.*, 1993, **70**, 958-961.
32. G. A. Sefler, Q. Du, P. B. Miranda and Y. R. Shen, *Chem. Phys. Lett.*, 1995, **235**, 347-354.
33. X. Gao, Y. L. Su, W. W. Zhao, Q. Y. Qian, X. Chen, R. Wittenbrink and D. J. Wang, *J. Phys. Chem. B*, 2017, **121**, 6659-6666.
34. I. Bitsanis and G. Hadziioannou, *J. Chem. Phys.*, 1990, **92**, 3827-3847.
35. S. K. Kumar, M. Vacatello and D. Y. Yoon, *Macromolecules*, 1990, **23**, 2189-2197.
36. J. Baschnagel and K. Binder, *Macromolecules*, 1995, **28**, 6808-6818.
37. A. van der Lee, L. Hamon, Y. Holl and Y. Grohens, *Langmuir*, 2001, **17**, 7664-7669.
38. P. Gin, N. Jiang, C. Liang, T. Taniguchi, B. Akgun, S. K. Satija, M. K. Endoh and T. Koga, *Phys. Rev. Lett.*, 2012, **109**, 265501.
39. G. Maurel, F. Goujon, B. Schnell and P. Malfreyt, *J. Phys. Chem. C*, 2015, **119**, 4817-4826.
40. J. Giermanska, S. Ben Jabrallah, N. Delorme, G. Vignaud and J.-P. Chapel, *Polymer*, 2021, **228**, 123934.